Acoustic seabed classification using QTC IMPACT on single-beam echo sounder data from the Norwegian Channel, northern North Sea

Ellen Johanne Eidem[a,*] and Knut Landmark[a,b]

[a]Norwegian Defence Research Establishment (FFI), Maritime Systems Division, PO Box 115, N-3191 Horten, Norway
[b]University of Oslo (UiO), Department of Informatics, PO Box 1072 Blindern, N-0316 Oslo, Norway

[*]Corresponding author. Tel: +4733033924; fax: +4733047834. E-mail address: ellen-johanne.eidem@ffi.no (E.J. Eidem)
Electronic mail: ellen-johanne.eidem@ffi.no (E.J. Eidem), knut.landmark@ffi.no (K. Landmark)

Abstract:
Sediment mapping is important for understanding the physical processes, the impact of human activity, and the conditions for marine life on the seabed. For this purpose, the seabed classification tool QTC IMPACT analyses statistical variations in single-beam echo sounder data. QTC was applied in a large and physically diverse area of the Norwegian Channel, between 59°30□N and 61°N, to produce a new sediment map and to verify the QTC algorithm. The results were interpreted using ground truth (grain size analyses of 40 gravity cores and five grab samples), multi-beam echo sounder bathymetry (MBES), and seismo-acoustic profiles. Surficial sediments were divided into five classes: (1) mud and silt, (2) a variety of clay, silt and sand, (3) sandy mud with gravel, (4) sand with gravel, and (5) clay and sandy clay. Along the Norwegian coast, where MBES imagery shows evidence of glacial erosion, the surficial sediment distribution is variable. The echo shape analysis of QTC did not produce a natural partition of the data, and statistical assumptions did not always hold. Sediment classification was therefore sensitive to the choice of cluster algorithm. However, QTC produced the most physically plausible results on a large scale compared to other cluster algorithms. Class boundaries were consistent with supporting data. One exception is a transition from muddy to sandy sediments not visible in seismo-acoustic data. A possible explanation is that seabed fluid seepage and water current erosion cause sand particle transport into the western part of the channel. The study confirms the capability of QTC in a complex environment, but there are some possible improvements.

Keywords: Acoustic seabed classification; Marine geology; North Sea; Norwegian Channel; Sediments; Single-beam echo sounder

Abbreviations:

ASC:	Acoustic seabed classification
BIC:	Bayesian information criterion
CTD:	Conductivity, temperature and depth
FFI:	Norwegian Defence Research Establishment
ML:	Maximum likelihood
MBES:	Multi-beam echo sounder
NC:	Norwegian Channel
NGU	Geological Survey of Norway
PCA	Principal component analysis
PDF:	Probability density function
QTC:	Quester Tangent Corporation
SBES:	Single-beam echo sounder
UiB	University of Bergen
UiO	University of Oslo

1. Introduction

Acoustic seabed classification (ASC) is a technology for mapping surficial seabed properties and sediment distribution with echo sounders (Anderson et al., 2008). The idea is that a change in sediment composition often implies a change in acoustic properties. This results in a systematic difference in the recorded echoes, provided the data have been corrected for extraneous influences, such as variable water depth or instrument settings. ASC may resolve fine variations in seabed properties with a high spatial resolution, which makes it a valuable complement to sediment sampling. Information about seabed composition is useful in a range of problems, including sonar performance prediction, the original purpose of this work, benthic habitat mapping and marine

DOI til publisert versjon / DOI to published version: 10.1016/j.csr.2013.08.001

resource management (Brown and Blondel, 2009; Ellingsen et al., 2002; Freitas et al., 2003; Haris et al., 2012), environmental monitoring (Medialdea et al., 2008; Wienberg and Bartholomä, 2005), and geotechnical engineering (Bartholomä, 2006). A scientific understanding of the physical processes that form the seabed is also a goal in itself, and new acoustic techniques for seabed mapping are instrumental to achieve this.

Physics-based ASC methods estimate seabed acoustical parameters by fitting simulated data to observations (De and Chakraborty, 2011; Snellen et al., 2011; Sternlicht and De Moustier, 2003). Such methods are sensitive to instrument calibration errors and theory errors. Statistical methods search the data for systematic differences between distinct seabed types (Amiri-Simkooei et al., 2011; Haris et al., 2012; Madricardo et al., 2012; Van Walree et al., 2005). Such methods use pattern classification algorithms (Hastie et al., 2009; Theodoridis and Koutroumbas, 2009) and work best where observations divide naturally into a set of discrete classes, the nature of which may not be fully known in advance. Empirical relations have been used to estimate mean grain size from e.g. measured echo energy (Van Walree et al., 2006), but it is not straightforward to link acoustical response with lithology. Sound scattering strength is sensitive to the seabed surface roughness (Jackson and Richardson, 2007), which may be influenced by coverage with benthic organisms and bioturbation, or sediment transport and attendant bedform development due to currents or ocean waves. As highlighted by e.g. Wienberg and Bartholomä (2005), an ASC system is best employed in conjunction with other data to avoid interpretational mistakes, particularly side scan sonar images (in their case) or multi-beam echo sounder (MBES) bathymetry.

The objectives of this paper are twofold. First, to present a new map of the surficial seabed composition in a large and physically diverse area of the Norwegian Channel (NC), northern North Sea, with water depths from 100 to 700 m. The primary tool has been the statistical ASC software QTC IMPACT (Preston et al., 2004), applied to single-beam echo sounder (SBES) data. QTC software is a widely used ASC tool which has proven successful in other studies (Bartholomä, 2006; Brown et al., 2011; Ellingsen et al., 2002; Freitas et al., 2011; Hamilton et al., 1999; Wienberg and Bartholomä, 2005). The second objective of the paper is to evaluate the QTC approach and result, including underlying assumptions, using an extensive supporting data set. Analysis of supporting data, especially ground truth (grain size analyses), is key to the interpretation and verification of the ASC results.

The paper first introduces the physical setting of the study area (Section 2). The established Quaternary stratigraphy, on which our interpretation of seismo-acoustic data is based, is briefly explained. Section 3.1 summarizes the data acquisition, in particular the pre-processing of the SBES data, and the preparation and analysis of the sediment samples. Section 3.2 examines the principles of the QTC method, which include a method for depth compensation of echoes, a data reduction step, and a clustering algorithm derived from Bayesian classification theory. Section 3.2.3 explains our approach to validate the QTC clustering algorithm. Section 4 presents the raw classification results, which required merging two datasets with different pulse lengths, and the results of the cluster validity analysis. The ASC method is an unsupervised one, so interpretation of the classes is subsequently done by comparison with the distribution of the sediment samples. The ASC classes are finally compared with parametric sonar profiles and geomorphology. Section 5 discusses the significance of the ASC results, the performance of QTC, and compares with previous work. The paper ends with the main conclusions from this work (Section 6).

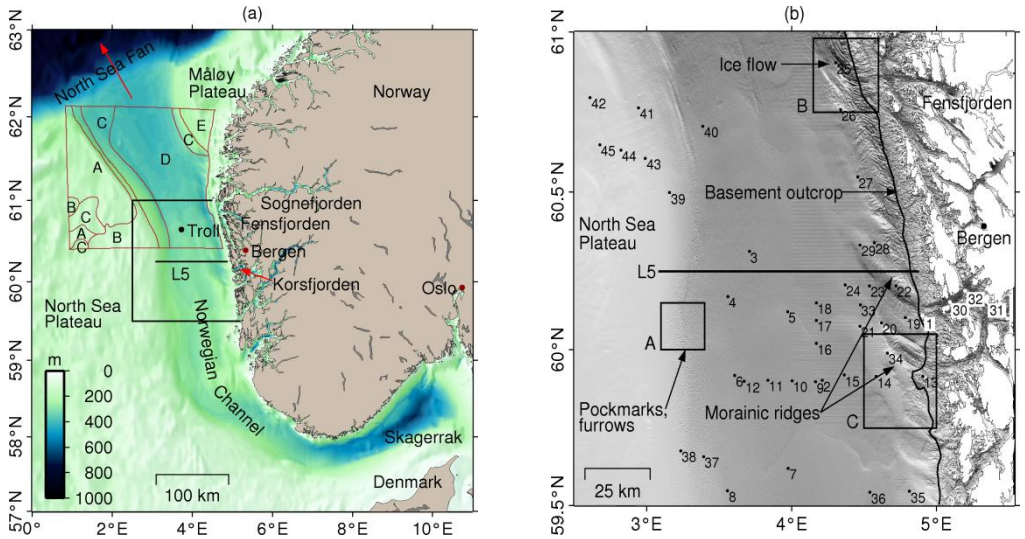

Fig. 1. (a) Overview and bathymetry of the Norwegian Channel. The study area to the west of Bergen is outlined. The Troll core is located at 60.64°N, 3.72°E. The brown polygons represent the sediment classes of Rise et al. (1984): sand with coarse material (A); very well-sorted sand (B); silty-clayey sand (C); silty, sandy clay (D); and variable (E). Map based on bathymetric data from (EMODnet, 2012), last accessed Dec. 2012). The line L5 is the transect of the seismic profile shown in Fig. 2. (b) Bathymetric relief of the study area based on MBES data, with principal morphological features indicated. The location of the 45 grain size analysed sediment samples (sample numbers given in Table 1) are also shown. The rectangular areas (A)–(C) are enlarged in Figs. 12 and 14.

2. Study area and seafloor geology

The NC is a depression in the continental shelf along the coast of southern Norway, with depths up to 700 m in the Skagerrak area (Fig. 1). It is a major topographic feature of the North Sea, which is a shallow continental sea bounded by the British Isles, Norway, and the northern European continent (Otto et al., 1990). The western slope of the NC is one of the major pathways for inflowing North Atlantic water. Mixed oceanic and fresh water flows out of the North Sea as the northbound Norwegian Coastal Current in the eastern and central NC (Winther and Johannessen, 2006). Thus the circulation pattern of the North Sea is influenced by the topography of the NC. Conversely, the NC is an important trap for water-borne sediments in the North Sea (De Haas et al., 1996).

The study area spans about 23 000 km^2 from the western Norwegian shoreline to the eastern margin of the North Sea plateau, between 59°30□N and 61°N latitude and to the east of 02°30□E (Fig. 1). The Quaternary sediments in this area consist of alternating layers of till and marine or glaciomarine sediments. The established Quaternary stratigraphy (Sejrup et al., 1995) is based in part on a drilled core sample (0–219 m below seafloor) from the Troll Field (Fig. 1). Of interest in this paper are the B1 unit and the A unit. Unit B1 is connected with seabed moraines in the eastern NC. Unit A is the top sediment layer in the central NC, truncated by the eastern moraines and, about 5–7 km from the shore, the crystalline basement (Fig. 2). Unit B1 is a till dating to the maximum of the Weichselian glaciation, corresponding to a homogenous diamicton in the Troll core with about 30% coarse material (grain size > 63 μm) and high shear strength (Andersen et al., 1995; Sejrup et al., 1995). Unit A is a horizontally bedded formation with sediments deposited from the onset of the last deglaciation to the present. The largest accumulations of unit A sediments are found outside the Korsfjorden inlet and at the foot of the North Sea Plateau (up to 60 m, compared to 17 m in the Troll core) (Fig. 3). The topmost layer in unit A, Holocene, has a variable thickness of typically 3–7 m as observed in present parametric sonar data (Fig. 3). In

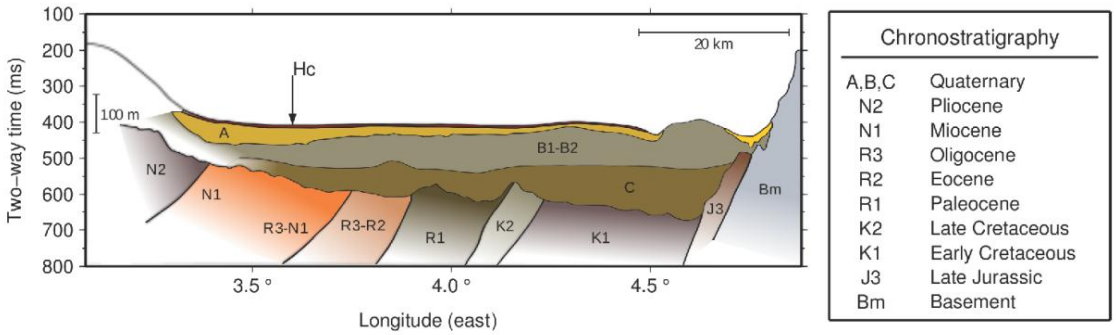

Fig. 2. Shallow stratigraphy (schematic) along seismic line L5 (Fig. 1). The interpretation is based on the stratigraphic work of Sejrup et al. (1995), Rise and Rokoengen (1984) and Sigmond (2002). The principal Quaternary units, all unconsolidated, are A (pelite), B1 (diamicton), B2 (sandy pelite over diamicton), and C (pelite). The topmost layer of unit A is a Holocene marine deposit (Hc). Crystalline basement (Bm) is exposed in the east, closest to shore. The total thickness of Quaternary sediments is about 150–200 m assuming a fixed average sound speed of 1800 m/s. The average sound speed has been estimated at 39 locations using seismic refraction and reflection data from sonobuoys (unpublished work by FFI). The vertical length scale has been calculated using 1800 m/s and is not accurate for the water or bedrock layers.

the Troll core, the topmost layer of unit A is a 4.5 m thick marine deposit consisting of silty clay with high water content (Andersen et al., 1995; Sejrup et al., 1995).

Rise and Rokoengen (1984) mapped the surficial sediments of the adjoining (partly overlapping) area between 60°30□N and 62°N, using seafloor photographs and sediment sample analyses. They divided the seabed sediments into four groups, from sand with coarse material to sandy clay (Fig. 1), and found increasingly more fine-grained sediments towards the central axis of the channel. Large local variations on the Måløy Plateau were interpreted as an effect of glacial activity.

3. Material and methods

3.1 Data acquisition and preparation

All the data were acquired by the Norwegian Defence Research Establishment (FFI), on FFI□s research vessel M/S H. U. Sverdrup II, during the years 2003–2008. The MBES was a 95 kHz Kongsberg Maritime EM 1002. The EM 1002 has 111 beams and 2° ×2° 3 dB beamwidth. The SBES was a 38 kHz Kongsberg Maritime EA 600 with a 3 dB beamwidth of 7.1°.

The SBES data were acquired using – arbitrarily – two pulse lengths (0.512 ms and 1.024 ms), and pre-processed with EchoView 4.40 (Myriax, previously SonarData, Tasmania). EchoView splits the raw data files into separate sonar (Sv–volume backscattering strength) and navigation files that can be read by QTC IMPACT. The transformation from raw data to backscattering strength consisted of automatically calibrating the data with respect to absorption factor (9.2–10 dB/km), transmit power (800–2000 kW), and sound speed (1500 m/s or as measured); the values used for each data file were as in the first ping. The absorption factor was computed according to the Francois and Garrison (1982) model. Further calibration factors were transducer gain, two-way beam angle, and 3 dB beamwidth (all user set). It was not possible to compensate for different pulse lengths. The SBES and MBES data were collected using a dense survey pattern with track line separation 500–600 m or less (full-coverage MBES surveys).

High-resolution seismic equipment (two 40 in^3 airguns with single-channel streamer) and a parametric sonar were used to map the Quaternary layer sequence. The parametric sonar was a Kongsberg Maritime Topas

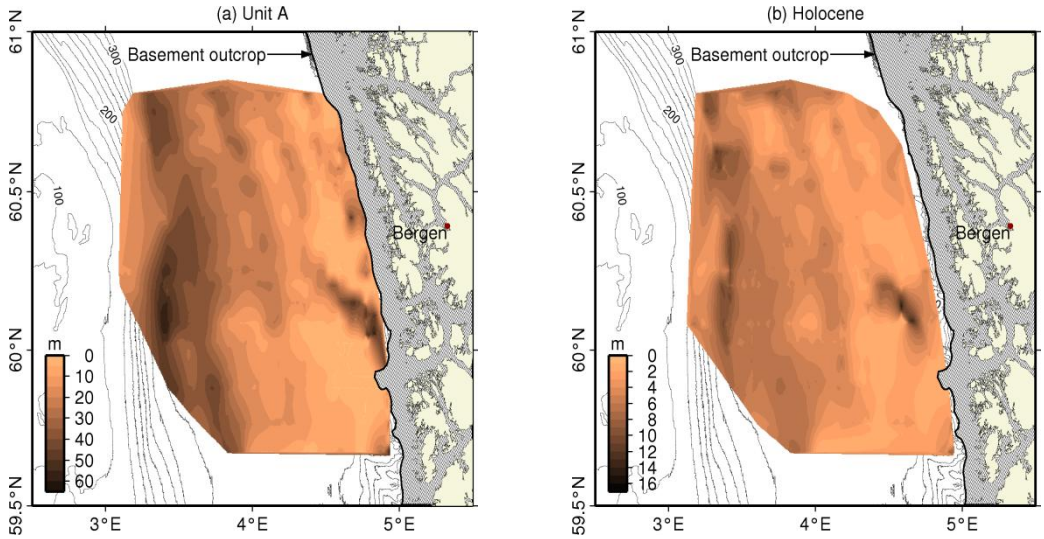

Fig. 3. Thickness (isopach maps) of unit A sediments in the Norwegian Channel based on interpretation of parametric sonar data (unpublished work by FFI). (a) Total thickness of unit A. Two-way travel time (seabed to top Weichselian moraine) was converted to meters using an average sound speed of 1550 m/s. (b) Thickness of surficial Holocene sediments, assuming an average sound speed of 1500 m/s. The interpretation of base Holocene was difficult in the western part of the channel. Seismic refraction analysis of sonobuoy data constrains the sound speed in unit A, but the uncertainty in the thickness estimates is at least 3–4%. For reference, bathymetric contours are also shown.

PS 018 transmitting a 20 ms 2–4 kHz chirp pulse. These data were acquired on a coarse survey grid with a total track length of about 2500 km. In total 39 sonobuoys were dropped during the seismic surveys to acquire wide-angle seismic data.

In total 40 single gravity cores with lengths between 0.4 and 2.8 m and a diameter of 63 mm were acquired at water depths of 170–670 m. Five grab samples were collected with a Van Veen grab sampler at water depths of 110–180 m. The sediment samples were sent to the University of Bergen (UiB) in four batches (2006, 2007 and two in 2008) for quantitative analyses. The gravity cores were analysed with respect to grain size distribution, sound speed, gamma density, shear strength and partly magnetic susceptibility. Only grain size distributions were obtained for the five grab samples. An additional 32 grab samples collected with the Van Veen grab sampler in the early phase of the study were analysed rudimentarily and given a qualitative description by FFI and the Geological Survey of Norway (NGU). The analysis was limited because the study was initially conceived mainly as an MBES survey program.

The UiB grain size laboratory analysis consisted of two steps. The cores were subsampled at ca. every 20–40 cm (2006–2007) and 4–85 cm (2008), and approximately 10–20 g samples were collected for each analysis. The samples were submerged in distilled water and agitated for 48–72 hours, before sieving through progressively smaller meshes: 1 mm, 0.25 mm (2008 only), 0.150 mm (2007 only), 0.125 mm, and 0.063 mm. The sediments collected on each sieve were dried and reweighed. The distribution of sediments smaller than 0.063 mm was analysed down to 2 μm (2006, 2008) and 1 μm (2007 only) using a Micrometrics Sedigraph 5100 (2006 only) and Micrometrics Sedigraph III 5120 (2007–2008). Nine of the ten core samples containing sediments coarser than 1 mm according to the first analysis, were re-sieved for classification purposes in 2008 using in addition a 2 mm mesh to establish the amount of gravel.

The grain size laboratory analysis of the five grab samples (2008) consisted of collecting and sieving approximately 100–400 g material of each sample. The meshes had sizes 4, 2, 1, 0.5, 0.25, 0.125 and 0.063 mm. One of the samples was analysed down to 2 μm using the Micrometrics Sedigraph III 5120.

Core and grab samples with less than 2% gravel were classified according to the Folk classification system (Folk, 1954), based on the grain size distribution. Sediment samples with at least 2% gravel were classified according to a modified version of the Folk classification system, where no division between 2 and 30% gravel exist, and the class gravelly, sandy mud (gsM) is introduced; consequently the original Folk class gravelly mud (gM) is reduced to cover samples containing maximum 10% sand and 30% gravel. The classification was performed on the top subsample of each core, with mean depth ranging from 1 to 16 cm. In average the mean depth was 5.8 ± 3.1 cm (the wavelength of the acoustic signals for a 38 kHz echo sounder is 4 cm). The classification is based on the mass percentage of gravel (grain size > 2.0 mm), sand (grain size 63 μm–2 mm), silt (grain size 2–63 μm), and clay (grain size < 2 μm). The sand and gravel content of all the subsamples at each site was calculated to find layers in the gravity cores; of special interest has been the composition of the surface layer.

3.2 Acoustic classification

QTC IMPACT analyses the shape of seabed echoes (Preston et al., 2004). The digitally sampled echoes are first aligned and summed over consecutive pings (stacking), a common noise reduction step. QTC has an automatic bottom detection algorithm for aligning echoes before summation. The shape analysis produces 166 parameters (features) which are stored in a feature vector ($\mathbf{x}$). A representative subset of feature vectors (the "catalogue data") is used to compute a principal component transform. By discarding all but three principal components, each observed feature vector is subsequently reduced to a data (observation) vector $\mathbf{d}(\mathbf{x}) \in \mathbb{R}^3$.

QTC IMPACT version 3.40 and 3.50 was used in this study. The stack length was five pings. Bad traces were manually removed using a built-in data editor. The reference depth was set to 300 m; the observed depth range was from 100 to 600 m. The data with pulse lengths τ=0.512 ms and τ=1.024 ms were processed separately. The several depressions (pockmarks) observed were not removed. The classified observations were decimated with a 200 m × 200 m block mode filter using Generic Mapping Tools (Wessel and Smith, 1991) and plotted along with ground truth data on shaded relief maps of MBES bathymetry for evaluation. Only blocks with a unique class were accepted. The classification results for the two pulse lengths were merged into one map in a similar process. Finally, the classes were given a sedimentological description based on classification of the 40 core and five grab samples.

3.2.1 Echo compensation

An echo time series depends on intrinsic properties of the seabed (roughness and volume scattering strength, reflection coefficient, sound attenuation), but also extraneous factors (source strength, receiver sensitivity, pulse length, frequency, beamwidth, propagation loss, water depth, and seabed slope). The QTC algorithm normalizes the stacked echoes to unit peak amplitude, so only echo shape is taken into account (Preston et al., 2004). Besides seabed slope, this leaves the effect of water depth on the echo length as the principal extraneous factor. The procedure to eliminate this factor is described in Preston (2005). Briefly, the echo length is parameterized by water depth D, beamwidth Ψ, pulse length τ, and sediment penetration depth. For a given frequency f, QTC computes a standard penetration depth p_{ref}. This is used to compute a reference echo length $T_{ref} = T_{ref}(D, \Psi, \tau; p_{ref})$, where D is the only parameter that varies from ping to ping. Each echo

Table 1. The location, water depth, core length (recovery), content of clay (< 2 μm), silt (2–63 μm), sand (63 μm–2 mm), and gravel (> 2 mm), median grain size, Folk class and QTC class (Turquoise, Yellow, Red, Brown and Purple) of the grain size analysed sediment samples. Samples #1–40 were obtained using a gravity corer; #41–45 using a grab. The grain size is expressed in $\phi = -\log_2(D)$, where D is the particle diameter in mm.

#	Lat (deg)	Lon (deg)	D (m)	L (cm)	Clay (%)	Silt (%)	Sand (%)	Gravel (%)	ϕ_{50}	Folk class[b]	QTC class
1	60.11	4.90	240	123	21.6	30.2	43.5	4.7	4.7	gsM	Outside
2	59.90	4.21	285	155	35.1	56.4	8.5	0.0	8.0	M	T
3	60.31	3.71	298	193	33.8	61.0	5.2	0.0	7.5	M	T
4	60.17	3.56	292	104	22.1	69.9	8.0	0.0	6.8	Z	T
5	60.12	3.97	279	126	31.5	66.6	2.0	0.0	7.9	Z	T
6	59.92	3.61	280	190	21.1	74.6	4.4	0.0	6.4	Z	T
7	59.62	3.98	274	276	51.3	47.4	1.3	0.0	9.1	M	T
8	59.55	3.56	247	190	28.0	59.6	12.3	0.0	6.2	sZ	T
9	59.90	4.17	277	182	18.1	78.3	3.6	0.0	6.8	Z	T
10	59.90	4.00	277	117	27.5	68.9	3.6	0.0	7.4	Z	T
11	59.90	3.84	283	114	17.0	81.7	1.2	0.0	7.1	Z	T
12	59.90	3.67	280	117	14.3	82.1	3.6	0.0	6.5	Z	T
13	59.92	4.91	199	42	23.4	21.7	49.2	5.7	3.3	gmS	Outside
14	59.91	4.58	243	198	15.0	30.4	52.0	2.5	3.4	gmS	R
15	59.92	4.36	283	204	33.0	45.1	13.2[a]	8.7[a]	7.7	sM?	T
16	60.02	4.17	283	157	34.0	63.2	2.8	0.0	8.1	M	T
17	60.09	4.17	291	167	41.5	55.8	2.7	0.0	8.5	M	T
18	60.15	4.17	294	138	33.7	63.9	2.4	0.0	8.1	M	T
19	60.10	4.78	321	208	36.0	50.1	14.0	0.0	8.1	sM	T
20	60.09	4.62	312	124	38.9	57.3	3.8	0.0	8.4	M	T(R)
21	60.08	4.47	274	193	28.3	35.6	36.0	0.0	6.8	sM	R
22	60.20	4.72	285	53	38.7	27.0	33.8	0.5	7.7	sM	R
23	60.20	4.54	315	149	28.8	68.1	3.1	0.0	7.6	Z	T
24	60.21	4.37	284	158	34.9	60.1	5.0	0.0	8.1	M	T
25	60.90	4.30	434	232	66.9	31.8	1.3	0.0	11.0	C	Y
26	60.76	4.34	326	119	20.6	13.1	62.0	4.2	2.7	gmS	Y
27	60.55	4.46	317	142	57.7	35.2	7.1	0.0	9.7	M	T
28	60.34	4.57	295	214	53.4	28.8	17.8	0.0	9.3	sM	R
29	60.33	4.47	275	148	35.7	19.0	42.3	3.0	5.9	gsM	Y
30	60.15	5.09	615	230	52.6	21.7	25.7	0.0	9.2	sC	P
31	60.10	5.49	590	163	65.1	34.4	0.6	0.0	10.3	M	P(R)
32	60.19	5.20	672	172	70.3	27.7	2.0	0.0	11.0	C	P(R,T)
33	60.14	4.47	289	149	64.0	31.8	4.2	0.0	10.3	C	P
34	59.99	4.66	236	51	29.0	11.7	50.7	8.5	2.6	gmS	R(Y)
35	59.55	4.81	211	44	28.9	16.6	40.0	14.5	3.5	gsM	R
36	59.54	4.54	260	56	19.4	12.0	43.0	25.6	2.1	gmS	R(Y)
37	59.66	3.39	220	90	13.2	58.7	28.0	0.0	4.6	sZ	T(Y)
38	59.68	3.23	168	237	45.5	50.4	4.1	0.0	8.4	M	T
39	60.50	3.16	168	143	35.0	39.3	25.7	0.0	6.6	sM	R
40	60.71	3.39	324	131	28.4	59.0	12.6	0.0	5.5	sZ	Y
41	60.76	2.94	184		3.3	9.3	87.0	0.5	3.4	zS	Y(R)
42	60.80	2.61	124		0.5[c]		66.1	33.4	0.9	sG	B(R)
43	60.61	2.99	139		25.9[c]		71.7	2.4	3.2	gmS	R
44	60.63	2.82	109		0.3[c]		92.0	7.8	2.3	gS	B
45	60.65	2.68	106		1.5[c]		98.5	0.1	2.4	S	B

[a]The sample was sieved using 1 mm mesh as maximum. The classification sM is assuming less than 2% gravel in the sample.
[b]The modified version of the Folk classification system is used for sediment samples with more than 2% gravel.
[c]The four grab samples were sieved using a 63 μm mesh as minimum.

is resampled at a rate $N / T_{ref}(D)$, where the fixed number of samples N is set by the operator. With respect to a reference depth D_{ref}, this resampling is equivalent to a depth-dependent time dilation $t \mapsto \left[T_{ref}(D_{ref}) / T_{ref}(D) \right] t$, whereby shallow echoes are stretched out in time and vice versa. This makes it possible to compare echo shapes at varying depths.

3.2.2 Unsupervised classification and statistical assumptions

The QTC algorithm is based on a normal mixture model (Preston et al., 2004; Preston and Kirlin, 2003). By assumption, the probability density function (PDF) for an observation $\mathbf{d}$ is

$$p(\mathbf{d}\,|\,\mathbf{q},\mathbf{w};c)=\sum_{j=1}^{c}p(\mathbf{d}\,|\,\omega_j,\mathbf{q}_j)P(\omega_j), \tag{1}$$

where $p(\mathbf{d}\,|\,\omega_j,\mathbf{q}_j)$ a normal PDF associated with the class denoted ω_j. $P(\omega_j)$ is the unknown prior probability or relative class frequency, and c is the number of classes. Here we let $\mathbf{q}_j$ denote the nine unknown parameters of $p(\mathbf{d}\,|\,\omega_j,\mathbf{q}_j)$ in three dimensions, and write $\mathbf{q}=\mathbf{q}_1\ldots\mathbf{q}_c$ and $\mathbf{w}=P(\omega_1)\ldots P(\omega_{c-1})$. The minimum-error Bayesian classification rule implies that $\mathbf{d}$ should be assigned to the class ω_i if the discriminant function

$$g_i(\mathbf{d})=\log p(\mathbf{d}\,|\,\omega_i,\mathbf{q}_j)+\log P(\omega_i) \tag{2}$$

is larger than $g_j(\mathbf{d})$ for all $j\neq i$ (Theodoridis and Koutroumbas, 2009). For a catalogue dataset of n observations, $\mathbf{D}=\mathbf{d}_1,\ldots\mathbf{d}_n$, QTC runs a stochastic optimization process, minimizing a cost function, to determine the unknown parameters $\mathbf{q}$ and $\mathbf{w}$. The cost function of QTC (Preston, 2009; Preston et al., 2004) will here be written in terms of Eq. (2), thus

$$E=-2\sum_{k=1}^{c}\sum_{i=1}^{n_k}g_k(\mathbf{d}_{ki}). \tag{3}$$

Here $\mathbf{d}_{ki}$ is the *i*th member of the *k*th class, and n_k is the number of observations currently assigned to the *k*th class (so $n=\sum_{k=1}^{c}n_k$). At every stage in the process, maximum likelihood (ML) estimates $\hat{\mathbf{q}}_j^{ML}$ and $\hat{w}_j^{ML}$ are computed using only the samples currently assigned to class ω_j. These estimates are accurate when the classes are well separated.

The number of classes is determined by repeating this process for different values of c to find the value that minimizes the quantity $E+M\log n$, where $M=\dim\mathbf{q}+\dim\mathbf{w}=10c-1$ is the number of free parameters. This maximizes the likelihood of c, given the data $\mathbf{D}$ and Eq. (1), but only under certain conditions that we will here make clear. From Eq. 8 in Bhat and Kumar (2010) and Duda et al. (2001) it follows that

$$-2\log \mathrm{P}(\mathbf{D}\,|\,\mathrm{c})\approx \min \mathrm{E}+\mathrm{M}\log \mathrm{n}. \tag{4}$$

The conditions are the following: (1) observations are independent; (2) $\log p(\mathbf{D}\,|\,\mathbf{q},\mathbf{w};c)$ has a global maximum and decays quickly; (3) there is no prior information about $\mathbf{q}$ and $\mathbf{w}$; (4) n is large; (5) no value of c is a priori more likely than others in the range we consider; and (6) $\min E=E(\mathbf{q}^{ML},\mathbf{w}^{ML})$, i.e. the true ML estimates are found. If $\min \mathrm{E}=\mathrm{E}(\mathbf{q}^{\mathrm{ML}},\mathbf{w}^{\mathrm{ML}})$, the right hand side of Eq. (4) is the Bayesian information

criterion (BIC), originally derived for models in the exponential distribution family (Schwarz, 1978). With all $g_i(\mathbf{d})$ finally determined from the catalogue data, the minimum-error rule is applied to classify all observations.

3.2.3 Cluster validation

Cluster analysis can be sensitive to the choice of algorithm (and input parameters), especially if the data do not form compact, well-separated clusters. We have applied three alternative clustering algorithms and used three cluster validity indices (Theodoridis and Koutroumbas, 2009) to measure the cluster compactness and separation as a function of c (the number of classes). The clustering algorithms were expectation-maximization (EM) with a normal mixture distribution, *k*-means, and self-organizing maps (SOM) (Kohonen, 1990; Theodoridis and Koutroumbas, 2009). The EM algorithm was chosen because it is related to the QTC algorithm. The validity indices were the global Silhouette index (Rousseeuw, 1987; Theodoridis and Koutroumbas, 2009), the Davies-Bouldin index DB_c (Davies and Bouldin, 1979), and the Dunn index D_c (Dunn, 1974). Each index is an overall cluster similarity (DB_c) or dissimilarity measure (S_c , D_c) for a given partition into *c* clusters. All three indices depend on a distance measure $\mathrm{r}(\mathbf{x},\mathbf{y})$ between pairs of observations $\mathbf{x}$ and $\mathbf{y}$. Here we used the Euclidean distance and a covariance-weighted distance. The latter was given as

$$\mathrm{r}(\mathbf{x},\mathbf{y})^2 = \left(\mathbf{x}-\mathbf{y}\right)^T \boldsymbol{\Sigma}^{-1}(\mathbf{x}-\mathbf{y}), \tag{5}$$

where $\boldsymbol{\Sigma}$ is the sample covariance matrix of all observations, with each observation given relative to it's own cluster mean. Ideally DB_c should be small ($DB_c \geq 0$), S_c should be close to 1 ($-1 \leq S_c \leq 1$), and D_c should be larger than 1. This signifies that the clusters are compact and well separated.

To check if the sample distribution of each class is compatible with the normal assumption, we used the fact that a normal PDF is on the form $p(\mathbf{d}\,|\,\omega_i) \propto \exp(-r^2/2)$, where r^2 is the squared Mahalanobis distance,

$$r^2 = (\mathbf{d}-\boldsymbol{\mu}_i)^T \boldsymbol{\Sigma}_i^{-1}(\mathbf{d}-\boldsymbol{\mu}_i). \tag{6}$$

Here $\boldsymbol{\mu}_i$ is the mean vector and $\boldsymbol{\Sigma}_i$ is the sample covariance matrix of the cluster to which $\mathbf{d}$ is assigned. For a multinormal distribution in K dimensions, r^2 follows a $\chi^2(K)$-distribution with K degrees of freedom. A relevant way to assess the QTC assumption is therefore to consider, for each class, a quantile–quantile plot of the empirical distribution of r^2 versus the $\chi^2(K)$-distribution (Johnson and Wichern, 1988). For a multinormal distribution, the observations are expected to lie on the line with unit slope.

4. Results

4.1 Sediment samples

Table 1 lists the location, water depth, core length (recovery), percentage of clay, silt, sand and gravel, median grain size, and the Folk class of the 45 top layer grain size analysed sediment samples (one sample per site). Most of the samples consisted mainly of fine sediments; 11 out of 44 samples contained more than 2% gravel, including one sample which contained more than 30% gravel. The sand content of the 11 samples with

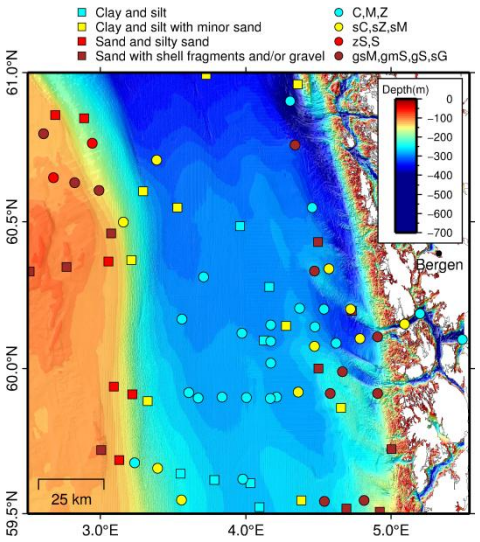

Fig. 4. The sedimentological and oceanographical diversity of the study area. The 45 grain size analysed sediment samples of the top layer (circles) and the 32 grab samples analysed rudimentarily (squares) are divided into four groups. Water depths greater than 400 m are plotted using a single color.

coarse sediments was higher than 40%. Of the remaining 33 samples, 22 contained less than 10% sand. One reason why the cores contained mostly fine sediments is that gravity core samples are difficult to obtain from hard, coarse seabeds.

The sediment samples from the central NC were classified mainly as silt (Z) or mud (M); mud is a mixture of silt and clay (Fig. 4). Two samples from the eastern part of the NC were classified as clay (C) and three samples retrieved at the foot of the North Sea Plateau as sandy silt (sZ). Grab samples from the North Sea Plateau contained 26–98% sand and 0–33% gravel; one grab sample was classified as pure sand (S). Sand and gravel was also found on the two southern morainic ridges to the east. Here the amount of gravel was 3–26%, which is higher than the amount of coarse material in the B1 unit of the Troll core (2–3% above 1 mm) (Sejrup et al., 1995). The amount of sand was 36–52%. Samples retrieved from the east-trending Korsfjorden were classified as clay (C), sandy clay (sC) and mud (M). Shell and shell fragments were observed in sediment samples from the North Sea Plateau. Dividing the 45 grain size analysed sediment samples into four groups based on the Folk class, and the 32 grab samples analysed rudimentarily into four equivalent groups based on the qualitative descriptions, demonstrates the diversity of the study area (Fig. 4). Although the rudimentary analysis is not precise enough to distinguish between all the Folk classes, this information both support and supplement the pattern observed from the grain size analyses. The median grain size, sometimes used to describe sediments (Freitas et al., 2003), ranges from 1ϕ to 11ϕ in the study area (Fig. 5a). Layers are present in the sediment cores that have top subsamples containing sand and gravel; typically the surficial sediments are coarser than beneath. Some cores show intermediate layers with increased sand and gravel content (Fig. 5b). The 22 sediment cores that have top subsamples with less than 10% sand show with two exceptions no dominant layers.

4.2 Acoustic classes and seabed types

The need to process two pulse lengths separately made the processing and analysis more complicated; two sets of statistics and classification rules had to be computed. The full dataset for each pulse length was used as catalogue data. The statistical clustering process (Section 3.2) was repeated for c in the range 4–8 (the number of

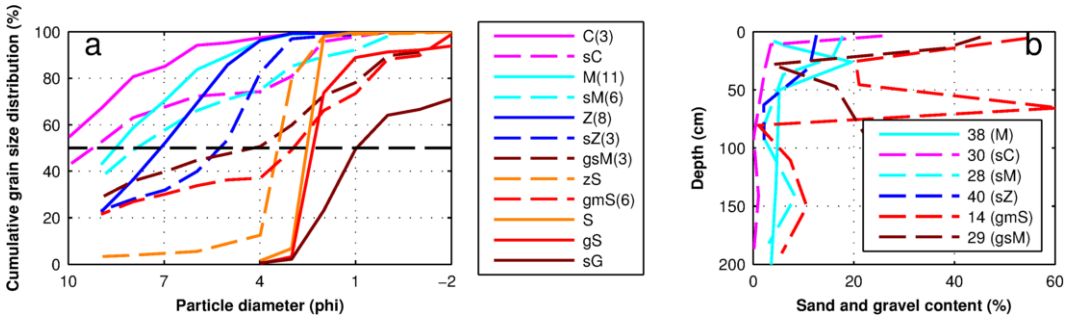

Fig. 5. (a) The average grain size distribution of top layer sediment samples with equal Folk class (the number of samples averaged in parenthesis). The grain size is expressed in $\phi = -\log_2(D)$, where D is the particle diameter in mm. Abbreviations: clay (C), mud (M), silt (Z), sandy clay (sC), sandy mud (sM), sandy silt (sZ), silty sand (zS), sand (S), gravelly sandy mud (gsM), gravelly muddy sand (gmS), gravelly sand (gS), and sandy gravel (sG). (b) Sand and gravel content versus depth in selected core samples.

classes). For a fixed value of c, the process was repeated 10 times with different random starting configurations. The number of classes (five) in the final ASC results was selected as the lowest number of classes where an increment of one did not change the pattern visually on a large scale.

The classification results for the τ=1.024 ms dataset (Fig. 6) show that one class covers most of the central channel. The slope on the western side is divided into two parallel classes which follow the bathymetric contours. The North Sea Plateau came out as one class. To the east all three classes observed in the west are mixed together, and the picture is more complex. There is also a fifth class close to the coast and in the fiords. The classification results for the τ=0.512 ms dataset (Fig. 6) show that the central NC is one class, just as for the τ=1.024 ms dataset. The moraines in the east stand out as one class, but with traces of other classes. There are three classes on the western slope and North Sea Plateau, just as for the τ=1.024 ms dataset.

The final classification results with an interpretation of the five acoustic classes are presented in Fig. 6 and show that there is good agreement between crossing legs, although some discrepancies occur. The joint geographical distribution of the five acoustic classes and the grain size analysed surficial sediment samples indicates a close correspondence. The turquoise class dominates the central channel with sediment samples classified as mud (M) and silt (Z). Four samples from this area are classified as sandy mud (sM) and sandy silt (sZ). The two sM samples are near the moraines, which may explain the content of coarser sediments (14% and 22% sand and gravel). The two sZ samples associated with the turquoise class are in the south-west portion of the study area; one is on the border with the area of yellow shading in Fig. 6, containing 28% sand and gravel, and the other is from the channel, containing 12% sand and gravel. Excluding these four core samples (#8, #15, #19, and #37, see Fig. 1b) the average content of clay, silt, sand and gravel is 33%, 63%, 4% and 0%, respectively. The average median grain size is 7.8ϕ. We note that a muddy (M) core sample (#38, see Fig. 1b) matches the turquoise class, which here extends up into the elsewhere sandy western slope. This core has a sandy layer revealed in the subsample at 26 cm depth (Fig. 5), with a sand content of 19% (less than 1% gravel). The sandy surface layer of the two sZ samples extends down to about 50 cm depth (the top subsamples are from 3 and 16 cm depth). The thickness of the sandy surface layer of the two sM samples (#15 and #19) has not been determined due to under-sampling. Far into the channel north-west of the northern moraine shell fragments were observed in two of the grab samples analysed rudimentarily only.

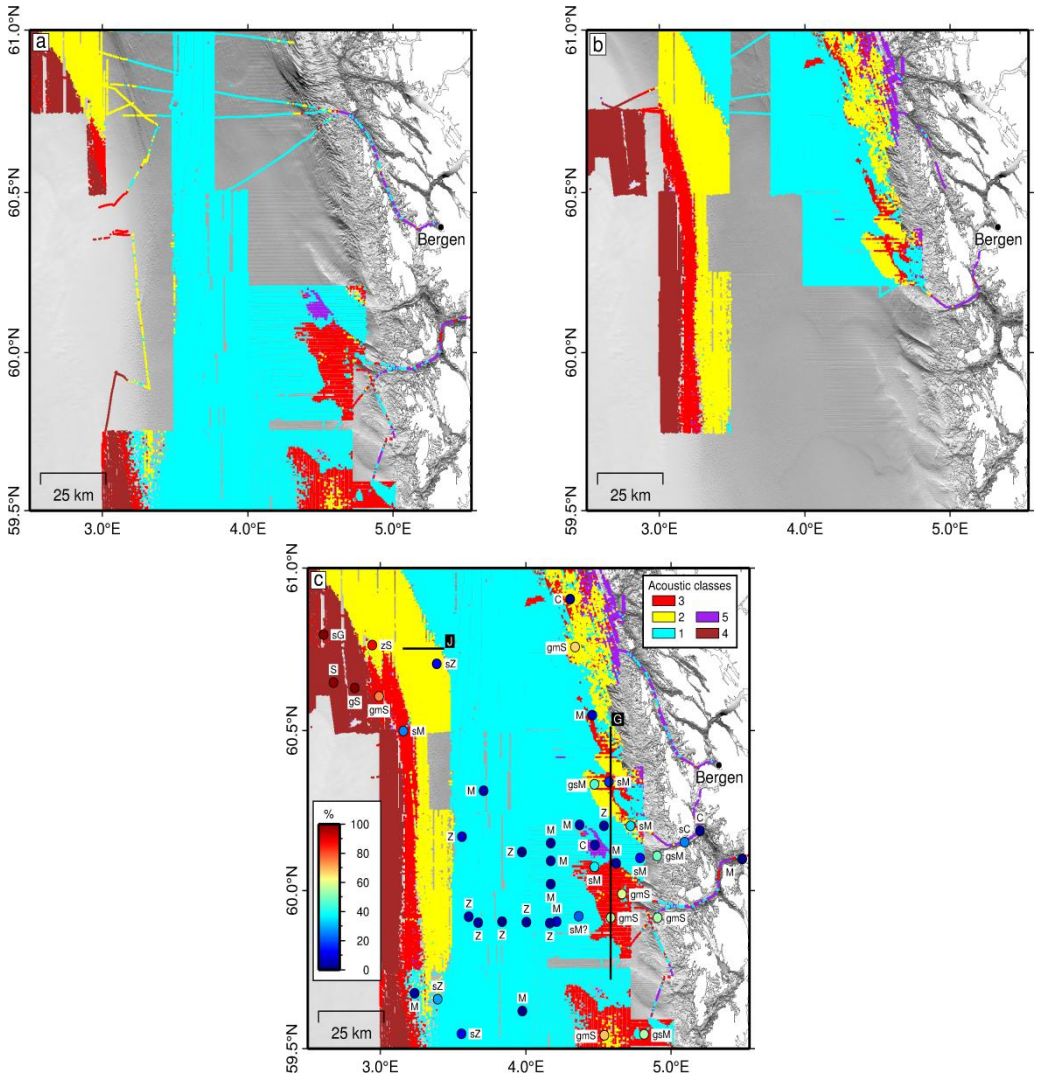

Fig. 6. The ASC results for pulse length τ=0.512 ms (a) and τ=1.024 ms (b). The colors have been deliberately chosen to match. The final classification results (c) include a qualitative description of the five classes: (1) mud and silt, (2) a variety of clay, silt and sand, (3) sandy mud with gravel, (4) sand with gravel, and (5) clay and sandy clay. The Folk class and content of sand and gravel of cores (top subsamples) and grab samples are shown for comparison; the color scale is in percentage. The parametric sonar survey transects G and J are indicated in black.

The red class covers the moraines, some small areas in the north-east, and a part of the western slope (shown as area of red shading in Fig. 6). The area contains a mixture of samples classified as sandy mud (sM), gravelly sandy mud (gsM), or gravelly muddy sand (gmS). Some rudimentarily analysed grab samples contain shells and shell fragments. The red class sediments are thus heterogeneous. The average median grain size of the five core samples from the two southern moraines (#14, #21, and #34–36) is 3.7ϕ; the average content of clay, silt, sand, and gravel is 24%, 21%, 44% and 10% respectively. We note that the four sM samples associated with the red class have median grain size values in the range of 6.6–9.3ϕ, and the sand content is 18–36% (less than 0.5% gravel). The fact that these four samples correspond with the red class suggests that presence of sand has a larger influence on the QTC results than the median grain size indicates. The cores associated with the red class typically have intermediate layers of coarser sediments (Fig. 5).

The yellow class is present both in the west and in the east. In the west the class extends from the slope into the deep channel, and the sediment samples associated with this class are classified as sandy silt (sZ) and perhaps

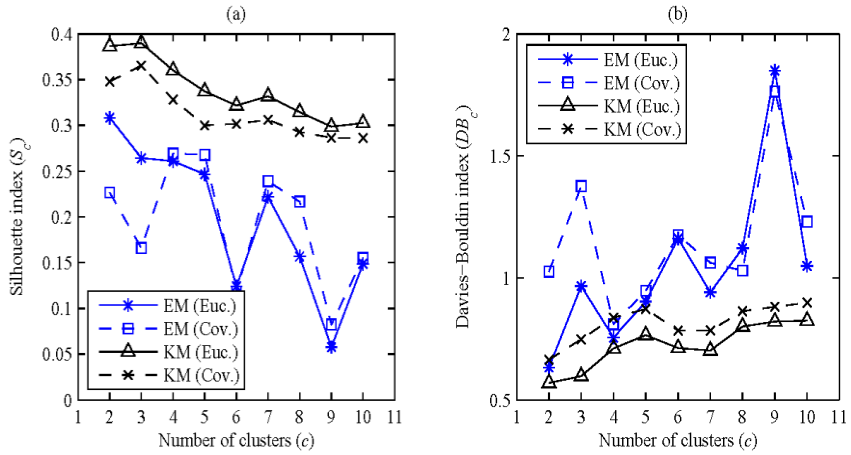

Fig. 7. Silhouette index (a) and Davies-Bouldin index (b) as a function of the imposed number of clusters for two different cluster algorithms, expectation maximization (EM) and k-means (KM). The indices were computed using both the Euclidean (Euc.) and covariance-weighted (Cov.) distance measures. A higher silhouette index S_c and a lower Davies-Bouldin index DB_c signify better separated and/or more compact clusters.

silty sand (zS). In the east the yellow class occurs in an area where the nature of the sediment samples is variable. The few samples from the homogeneous parts of the yellow class make the analysis of sediment content uncertain. The most dominant tendency is only 0–4% gravel. The percentage of clay, silt, and sand varies a lot. There is also a large variability in depth, sometimes no layering and sometimes several layers in the upper 75 cm. The sandy surface layer of the sZ core sample from the north-western channel (#40, see Fig. 1b) is about 50 cm thick (Fig. 5b).

The brown class dominates the North Sea Plateau, and based on the classification of the three sediment samples associated with this class (#42, #44 and #45, see Fig. 1b), the seabed consists of sand and coarser sediments (including shells and shell fragments). The average median grain size is 1.9ϕ, and the average contents of sand and gravel are 86% and 14%, respectively. The mud content is less than 1%.

Both pulse lengths were used when surveying two of the fiords, and the purple class consistently dominates these. A small area in the channel at about 60.15°N, 4.5°E and a part of the glacially eroded zone in the NE were also assigned to the purple class. The four sediment samples from the area of purple shading in Fig. 6 contains fine sediments and were classified as clay (C), sandy clay (sC), and mud (M). The average content of clay, silt, sand, and gravel is 63%, 29%, 8% and 0% respectively. The average median grain size is 10.2ϕ. Even though the clay (C) core sample from the channel (#33, see Fig. 1b) also matches the purple class, the surficial clay layer is thin. The clay content of the second to top subsample (5 cm deeper) is lower (55% compared to 64%); this subsample is classified as mud (M). The sandy surficial layer is also thin in the sC core sample from the fiord (#30, see Fig. 1b); the second to top subsample (7.5 cm deeper) contains only 3.5% sand (compared to 25.7% sand in the top subsample).

4.3 Cluster validity

To compute the cluster validity indices (Fig. 7), the EM algorithm (with normal components), *k*-means, and the SOM method were applied to a subset of 10 000 randomly selected observations. Here we summarize the results for the $\tau = 0.512$ ms dataset. The validity indices for the τ=1024 ms dataset lead to similar conclusions. The sediment class map obtained with the SOM algorithm did not show good consistency with supporting data

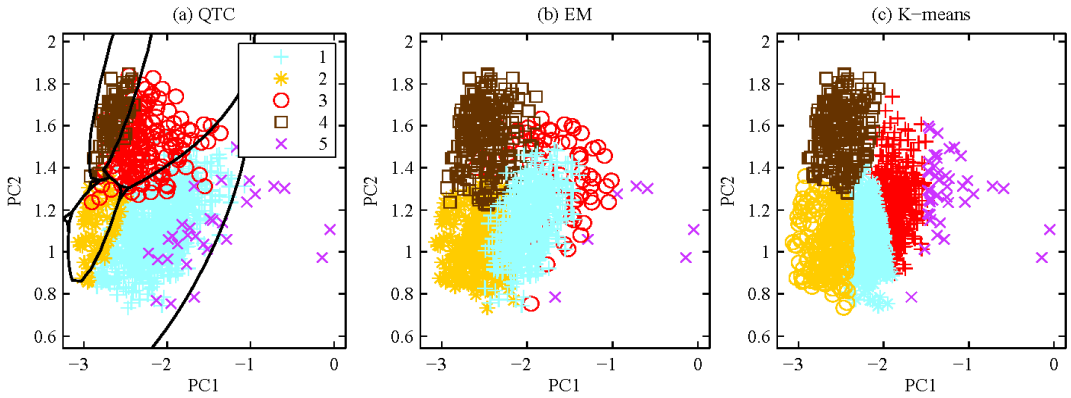

Fig. 8. Scatter plots of the two principal components (PC1 and PC2) for 1200 randomly selected observations after partition into five classes with QTC clustering (a), EM clustering (b), and *k*-means (c). The plot of the QTC clustering also shows the decision boundaries (points of equal posterior probability) obtained by considering only the two principal components.

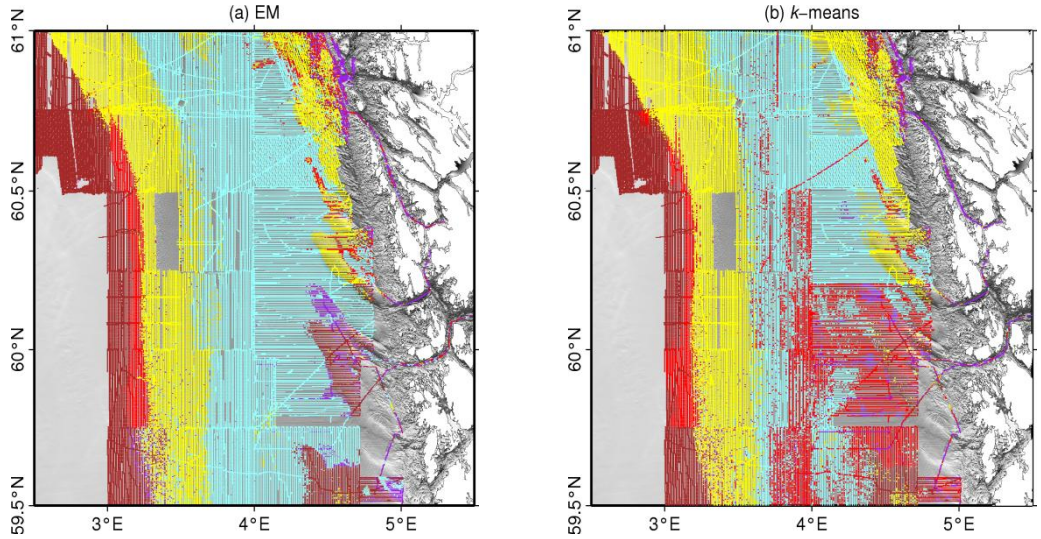

Fig. 9. Classification result (both pulse lengths combined) using EM clustering (a) and *k*-means clustering (b). These maps should be compared with the QTC results in Fig. 6.

compared to the QTC, EM, and k-means algorithms. There are several parameters in the SOM algorithm that can be tuned to improve the results, but we have instead omitted the validity indices for this algorithm (although they also point to the same conclusions).

The Dunn index DI_c was close to zero in all the experiments, which indicates that at least one pair of clusters are adjacent and poorly separated, although DI_c is sensitive to outliers. The lack of a knee or clearly optimum c -value in the graphs of Fig. 7, and the relatively good score for $c = 2$, also suggest that there is no clear cluster structure in the data. If we exclude $c = 2$ and $c = 3$ on physical grounds, as these values cannot account for the variation in the sample dataset, then four or five classes appear to be the overall best choices. The validity indices of the final QTC clustering with five classes are close to those of the EM method: $S_5 = 0.25$, $DB_5 = 0.88$ with Euclidean distances, and $S_5 = 0.25$, $DB_5 = 0.86$ with covariance-weighted distances.

Scatter plots of the two principal components for three different clusterings also suggest a lack of a clear cluster structure (Fig. 8). The overlap between the classes (particularly for QTC and EM) shows the importance of the third principal component. There are marked differences between the three clusterings (the SOM result was even more different). We have used the same colors in all three plots to ease comparison, but the physical

DOI til publisert versjon / DOI to published version: 10.1016/j.csr.2013.08.001

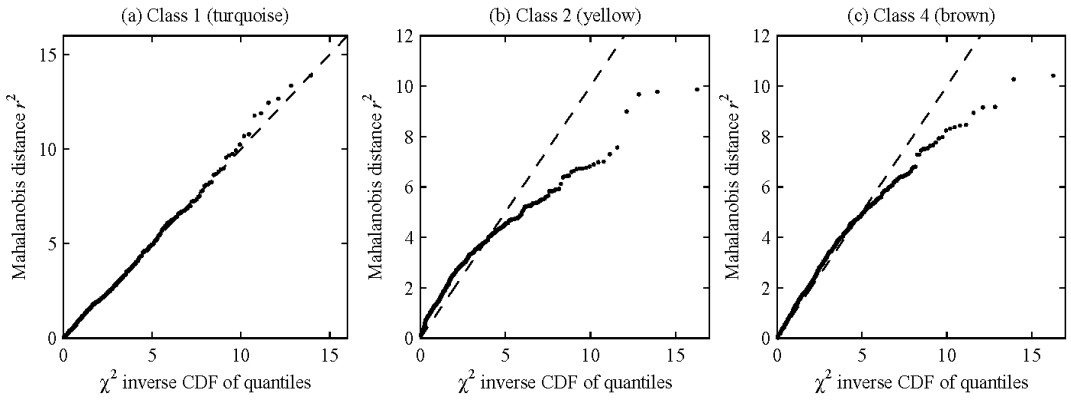

Fig. 10. Quantile-quantile plots of the observed Mahalanobis distance r^2 versus the χ^2 distribution with three degrees of freedom for 500 randomly selected observations per class. (a) turquoise class, (b) yellow class, and (c) brown class. For a multinormal distribution, the observations are expected to lie on the line with unit slope (dashed line).

interpretation of each color (class) will of course not be the same. This is evident in the class maps (Fig. 9), which have been processed in the same way as above using a $200\ \mathrm{m} \times 200\ \mathrm{m}$ block mode filter. The lack of cluster structure partly explains why the result is sensitive to the choice of algorithm. However, there are some features that are preserved, particularly the western boundary between the brown and yellow classes. The EM algorithm reproduces many of the features of the QTC result. For the τ=1.024 ms dataset, the QTC and EM class maps are almost indistinguishable.

For the final QTC result with five classes, the observed Mahalanobis distances (r^2) were sorted in ascending order and plotted against $F^{-1}(p_i, K)$, where $p_i = (i - 0.5)/n,\ i = 1, \ldots, n$ are n equally spaced quantiles, and F^{-1} is the inverse cumulative distribution function for $\chi^2(K = 3)$ (n is the number of observations). The quantile-quantile plots (Fig. 10) show that observations from the brown and yellow classes are not normally distributed, whereas the normal assumption is tenable for the turquoise class. The observations from the red and purple classes also deviate from the unit slope line, but less than for the brown and yellow classes. Note that removing suspected outliers did not improve the fit to the unit slope line.

4.4 Comparison with parametric sonar data and geomorphology

The ASC results were compared with parametric sonar profiles along several transects. There are clear changes in acoustic signature as the terrain shifts from horizontally bedded marine or glaciomarine sediments to morainic ridges. Comparing Figs. 3, 6 and 11, it is clear that the turquoise class in the central and eastern areas corresponds well with top unit A. The purple class matches a thinner layer (about 2–8 m thick) overlying the Weichselian moraine (Fig. 11, profile labelled G in Fig. 6). The top sediment sample from this layer was classified as clay.

The moraines on the eastern side of the channel have visible iceberg plough marks, as well as north-south-oriented parallel lineaments probably caused by a moving glacier (Fig. 12). The preservation, up through the Holocene, of traces of glacial erosion suggests two things: the marine sedimentation rate is low, and the seabed sediments have high stiffness. This is consistent with the interpretation of the red class (Fig. 6), and the boundary of the red class follows the outline of the moraines closely in the south-east (Fig. 11). Further north both the red

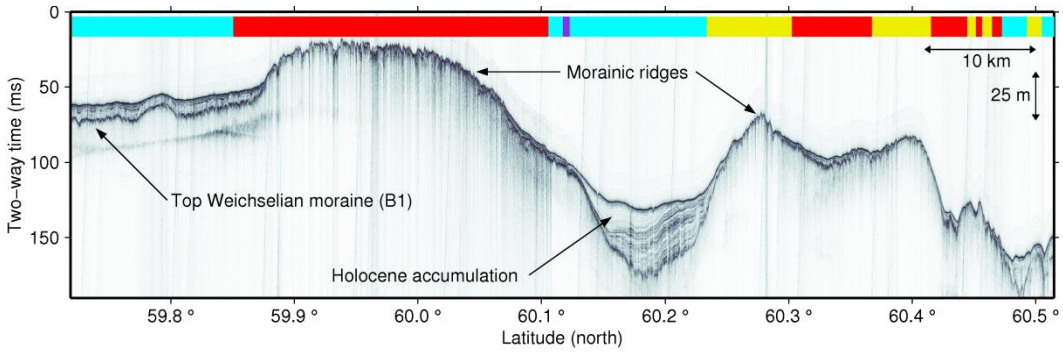

Fig. 11. Parametric sonar profile labelled G in Fig. 6 (instantaneous amplitude after deconvolution). The QTC classes are indicated with color bars. The vertical length scale is based on a sound speed of 1550 m/s, hence most accurate for unit A.

and yellow classes occur and both correspond with the Weichselian till (unit B1). It is difficult to distinguish between these two classes based on parametric sonar data alone.

The westernmost part of unit A corresponds with the yellow class. A comparison of the ASC results with a parametric sonar profile (Fig. 13, profile labelled J in Fig. 6) shows that the transition from dominantly muddy to dominantly sandy surficial bottom sediments occurs well into the unit A area. The top subsample of the nearby gravity core from 60.71°N, 3.39°E was classified as sandy silt (sZ) with a substantial sand fraction (13%), which confirms the presence of sand in the western NC (Fig. 6). The morphology of the western slope of the channel is a fluted pattern of elongated depressions (Fig. 14).

5. Discussion

Overall, the merging of the ASC results from the two data sets (τ=0.512 ms and τ=1.024 ms) shows a good match between the two. However, south and north on the western slope the correspondence between the red classes from the two datasets is reduced. There is also some disagreement between the red and brown classes in the north-western portion of the study area, on the North Sea Plateau. In order to improve the matching, a manual clustering may be beneficial; this has not been investigated in the present study.

The final ASC map based on SBES data and interpretation of supporting data (Fig. 6) gives a unifying and generally coherent picture of our observations, consistent with what we know about depositional and erosional processes in the region. Geographically and lithologically, the brown class corresponds well with class B of Rise and Rokoengen (1984), the yellow class corresponds with their class C, and the turquoise class corresponds with their class D (Section 2 and Fig. 1a).

In the north-east, the signs of massive glacial erosion, and probable presence of glacigenic sediments, explain why the ASC results are variable, with the red and yellow classes as predominant.

The ASC results were decimated with a 200 × 200 m block mode filter which removed fine-scale variations. The lack of consistency between the grain size analysed sediment samples associated with the yellow class may be explained by local variations in the seabed types in the north-east. The variable geomorphology also suggests that analyses of smaller regions are needed to understand the correspondence between the classification results and point sampling of the seabed. On the other hand, the QTC results may reflect more than simply the distribution patterns in sediment grain size, as stated by Wienberg and Bartholomä (2005).

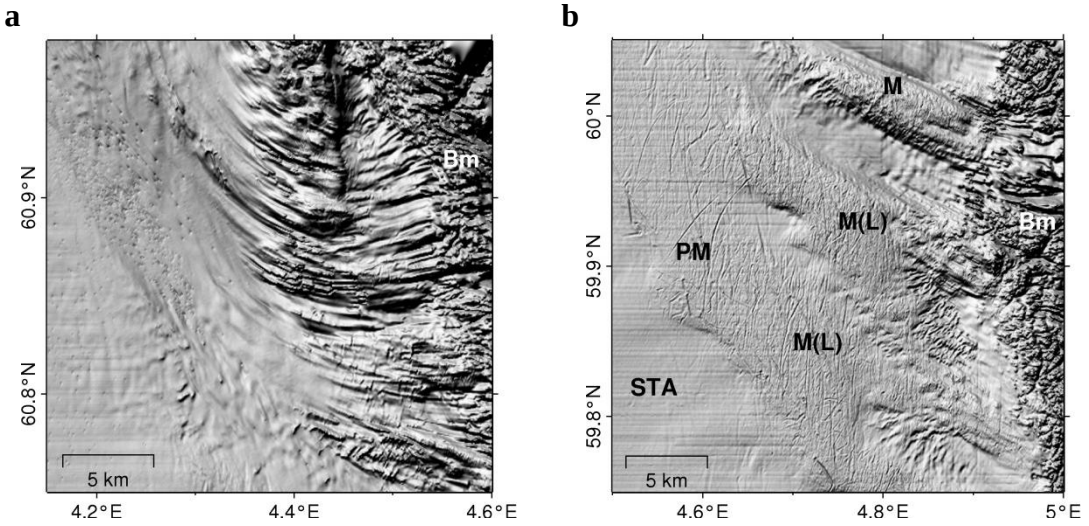

Fig. 12. Traces of glacial erosion on the eastern side of the study area (bathymetric relief based on MBES data). (a) The concentric patterns outside the Sognefjorden and Fensfjorden inlets suggest a movement of ice from the mainland and into the northbound Norwegian Channel Ice Stream. (b) Morainic ridges with glacial lineaments and plough marks extend north-west from the coastal zone, where basement is exposed at the seafloor. The figures are enlarged versions of area B and area C shown in Fig. 1b. Annotation: M: moraines; PM: plough marks; L: lineaments; Bm: basement; STA: ship track artifacts (parallel east-west-oriented lines).

The flow-like pattern seen outside the Sognefjorden and Fensfjorden inlets (Fig. 12b) suggests that this was a drainage area for the mainland ice sheet, where ice moved into the channel and was deflected northwards by the NC ice stream. Rise et al. (2004) observed a pattern of semi-parallel lineations on a deeper Quaternary horizon, immediately to the north of 61°N, which they believed to be caused by a mid-Pleistocene glaciation. The observations of Rise et al. (1984) too suggest a movement of ice from the mainland north-eastwards into the channel. On the western slope, the orientation of the elogated depressions (predominantly north-south) matches the direction of inflowing Atlantic water (Fig. 7). Bøe et al. (1998) interpreted similar patterns on the southern slope of the Skagerrak as current-modified pockmarks. Hovland (1983) observed very shallow gas blankets in boomer seismic data from a part of the western slope. There were apparent vertical escape routes matching the occurrence of elongated depressions in the seabed. He concluded that vertically migrating gas is lifting sediments into suspension above the escape routes; the suspended sediments are subsequently transported away by water currents. This mechanism may explain why the yellow class extends into the deep channel where we expected the turquoise class to dominate. Sand particles may accumulate on the seabed at the bottom of slope, and in decreasing amounts towards the center of the channel. The pre-Holocene part of unit A would be unaffected by this process, as it is a marine transport phenomenon. As observed in Sections 4.1 and 4.2, there is a sandy surface layer (about 50 cm thick in core #38), overlying finer sediments, in cores from this area. We therefore think that ASC gives the correct indication, even though this is not evident from the parametric sonar (or seismic) data. The sharp class boundary of the ASC map is however misleading if the transition is continuous. This demonstrates a basic limitation of the method. In general there may be observations that have low likelihood with respect to all classes.

The purple class present to the north of the moraines at 60.15°N, 4.5°E stands out (Fig. 6). There are no particular bathymetric features that might explain why this area is assigned to another class than the surroundings. The one sediment sample deliberately collected here based on initial ASC results, contains finer surficial sediments than neighbouring sediment samples. In a study by Van Vossen et al. (2013) this area also

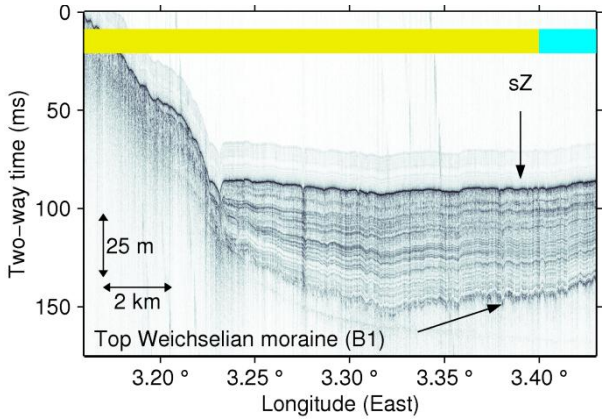

Fig. 13. Parametric sonar profile from the north-west side of the study area, labelled J in Fig. 6 (instantaneous amplitude after deconvolution). The QTC classes are indicated with color bars. The topmost layer of unit A (Holocene) appears homogeneous with little internal diffraction. A nearby gravity core shows a sandy surficial layer with the top-subsample classified as sandy silt (sZ). The vertical length scale is based on a sound speed of 1550 m/s, hence most accurate for unit A.

stood out from its surroundings. They applied a physics-based method to low-frequency sonar data acquired at 1–2 kHz. It was found that the area generally had lower reflection coefficient (at 7° grazing angle), as expected, but higher backscattering strength than the adjacent area of turquoise shading (Fig. 6).

The lack of a clear cluster structure in the echo shape data may partly be explained by a continuous change in seabed composition along the transverse axis of the channel. However, we have found no significant differences in the class distributions when comparing data from the eastern and western sides of the study area. The question is if there are other echo features that might give better class discrimination. Several aspects of the QTC method appear to be motivated by a need to make the software robust and straightforward to use. This makes sense given the amount of tuning and level of expertise often required to successfully run scientific codes, but it also introduces some limitations. For example, normalizing echo amplitudes eliminates the need to compensate for sound attenuation in the water column and to calibrate the acoustic signals. However, the total backscattered energy is then lost, a potentially useful feature (Van Walree et al., 2006; Van Walree et al., 2005) . Likewise, restricting the analysis to three principal components avoids all the problems of classification in high dimensions (Hastie et al., 2009), and limits the amount of catalogue data needed to make robust PDF estimates, but this restriction too sheds potentially useful information. An alternative is to use aligned, digitally sampled echoes as feature vectors directly (Hamilton, 2011; Hamilton and Parnum, 2011) (each sample a feature). For such an approach we propose to use a piecewise constant function approximation (Jensen and Solberg, 2007) to reduce the number of features before running the classification algorithm.

Even if one uses all information inherent in a (stacked) echo, there are other potentially useful features. In their evaluation of QTC, Hamilton et al. (1999) suggested that some measure of variability within a set of pings might be useful for identifying rock or coral bottoms, where ping-to-ping fluctuations are large. More generally, our understanding is that QTC (the single-beam variant) does not take into account the statistics of a set of contiguous observations, and the classification process proceeds without information about spatial relationships, i.e. spatial location and neighboring observations do not affect the prior probabilities. We have not explored these possibilities in this work, but think that better classification accuracy may be achieved by using spatial information.

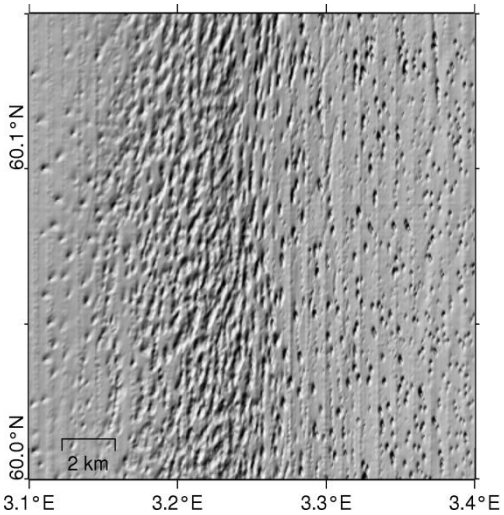

Fig. 14. Seabed morphology of area A (see Fig. 1). The western slope of the NC has an irregular, fluted pattern of elongated depressions, a possible sign of erosion by water currents and fluid seepage. The seabed of the deep part of the NC is flat but pockmarked. Parallel north-south-oriented ship track artefacts are also visible.

A fundamental limitation concerns the mapping of sloping areas. The scattering strength changes significantly with incidence angle in the near-nadir regime (except for very rough surfaces). If the seabed is sloping, the symmetry of vertical ensonification is destroyed, and this affects the echo shape. Using QTC, Von Szalay and McConnaughey (2002) found that slopes exceeding 5–8° caused the classification accuracy to break down. In the study area slopes of such magnitude only occur in the narrow basement zone and along the sides of the fiords, at least on a spatial scale of 50 m or more (the resolution of the terrain model that we have used). Except for a small area to the north-east we do not have ASC results from the basement zone. The only class that could potentially be affected by slope errors is the purple class. Pockmarks were not removed in the pre-processing step, and it should not be necessary. The use of a block-mode filter, which picks out the most frequently occurring class within a rectangular window (block), also helps to reduce such errors. The best solution we can think of to overcome the problem of steep slopes would be to transfer the echo shape methodology to an MBES system, and at any time apply it to the beam for which the true incidence angle is closest to zero.

If there is no obvious cluster structure, as in the present data, practical considerations may limit the number of classes. When the data distribution is not unimodal, the approximation $\mathrm{BIC} \approx -2\log p(\mathbf{D}\,|\,c)$ may be a poor one. We do not know if condition 2 [following Eq. (4)] holds. Moreover, the fact that classes are not well separated induces errors in the ML estimates during the cluster process. If two seabed types have overlapping PDFs, and the two types are unequally represented in the data set, the larger class may steal members from the smaller because of unequal priors. This is another argument for including spatial information in the classification process to adjust the priors depending on location. The non-normal distribution of some classes favours increasing c to fit the data. This may explain why the BIC decreased when c was increased beyond that which supporting data indicated. Nevertheless, the parsimony term $M \log n$ counters the tendency to overfit the data in any circumstances, and there are empirical reasons to use the BIC for normal mixtures (Roeder and Wasserman, 1997).

While QTC results were very similar to those of the simpler iterative EM algorithm, a qualitative comparison with supporting data has shown that QTC performed better than the *k*-means and SOM algorithms. Despite the above reservations, this provides support for the QTC algorithm as applied to a difficult data set.

6. Conclusions

We have used a statistical classification method (QTC IMPACT) for single-beam echo sounders to map the surficial sediments in the Norwegian Channel. The unsupervised classification results were interpreted in view of 40 gravity cores and 37 grab samples distributed across the whole survey area, MBES bathymetry and parametric sonar data. The ASC analysis has resulted in a high-resolution map where the seabed is divided into five classes: (1) silt and mud (deep, central channel), (2) a variety of clay, silt and sand (mainly north-east and lower western slope), (3) sandy mud with gravel (mainly moraines and upper western slope), (4) sand with varying amounts of gravel (predominant on North Sea Plateau), and (5) clay and sandy clay (inside fiords and one small area in the channel). The acoustic classification is highly sensitive to the sand and gravel content of the top layer. The five classes reflect the diverse erosional and depositional processes of the area, past and present: Glacial erosion on the eastern side, fluid seepage and water current erosion on the western side, and deposition of fine-grained suspended sediments in the central part.

The consistency of the results, across a large and diverse area, with respect to supporting data, different pulse lengths, and intersecting ship tracks, shows that QTC IMPACT is a reliable tool for sediment mapping. However, the lack of cluster structure in the set of observation vectors implies a degree of arbitrariness in the final classification result. This is partly due to the nature of sediment deposition in the study area, but also suggests that additional features should be introduced for better discrimination between Folk type classes. The study also highlights the need for careful verification and cluster validity analysis of results obtained by statistical ASC methods in general.

Acknowledgements

The authors acknowledge the scientific and technical crew of the research vessel M/S H.U. Sverdrup II for their efforts in collecting the large amount of data in this study. We thank Prof. Anne Schistad Solberg (UiO) and Dr. Paul van Walree (FFI) for reviewing drafts of this manuscript, and Prof. Haflidi Haflidason and his team (Department of Earth Science, UiB) for the laboratory analyses. We thank the Geological Survey of Norway for good advice, especially Dr. Ole Christensen (presently at Statoil) and Dr. Aivo Lepland, who assisted us on board the ship on two occasions and provided guidance on sediment classification. The work was financed by FFI, UiO and the Research Council of Norway (project Acoustic Image Formation and Interpretation).

References

Amiri-Simkooei, A.R., Snellen, M., Simons, D.G., 2011. Principal component analysis of single-beam echo-sounder signal features for seafloor classification. IEEE Journal of Oceanic Engineering 36 (2), 259–272.

Andersen, E.S., Østmo, S.R., Forsberg, C.F., Lehman, S.J., 1995. Late- and post-glacial depositional environment in the Norwegian Trench, northern North Sea. Boreas 24, 47–64.

Anderson, J.T., Van Holliday, D., Kloser, R., Reid, D.G., Simard, Y., 2008. Acoustic seabed classification: current practise and future directions. ICES Journal of Marine Science 65 (6), 1004–1011.

Bartholomä, A., 2006. Acoustic bottom detection and seabed classification in the German Bight, southern North Sea. Geo-Marine Letters 26, 177–184.

Bhat, H.S., Kumar, N., 2010. On the Derivation of the Bayesian Information Criterion, http://nscs00.ucmerced.edu/~nkumar4/BhatKumarBIC.pdf.

Brown, C.J., Blondel, P., 2009. Developments in the application of multibeam sonar backscatter for seafloor habitat mapping. Applied Acoustics 70 (10), 1242–1247.

Brown, C.J., Todd, B.J., Kostylev, V.E., Pickrill, R.A., 2011. Image-based classification of multibeam sonar backscatter data for objective surficial sediment mapping of Georges Bank,Canada. Continental Shelf Research 31, 110–119.

Bøe, R., Rise, L., Ottesen, D., 1998. Elongate depressions on the southern slope of the Norwegian Trench (Skagerrak): morphology and evolution. Marine Geology 146, 191–203.

Davies, D.L., Bouldin, D.W., 1979. A cluster separation measure. IEEE Transactions on Pattern Analysis and Machine Intelligence 1 (2), 224–227.

De, C., Chakraborty, B., 2011. Model-based acoustic remote sensing of seafloor characteristics. IEEE Transactions on Geoscience and Remote Sensing 49 (10), 3868–3877.

De Haas, H., Okkels, E., Van Weering, T.C.E., 1996. Recent sediment accumulation in the Norwegian Channel, North Sea. Norges Geologiske Undersøkelse Bullentin. 430, 57-65.

Duda, R.O., Hart, P.E., Stork, D.G., 2001. Pattern Classification, second ed. Wiley-Interscience.

Dunn, J.C., 1974. Well separated clusters and optimal fuzzy partitions. Journal of Cybernetics, 4, 95–104.

Ellingsen, K.L., Gray, J.S., Bjørnholm, E., 2002. Acoustic classification of seabed habitats using the QTC VIEW system. ICES Journal of Marine Science 59, 825–835.

EMODnet, 2012. European Marine Observation and Data Network,The European Commision. http://www.emodnet-hydrography.eu.

Folk, R.L., 1954. The distinction between grain size and mineral composition in sedimentary-rock nomenclature. Journal of Geology 62 (4), 344–359.

Francois, R.E., Garrison, G.R., 1982. Sound absorbtion based on ocean measurements: Part II: Boric acid contributions and equation for total absorbtion. Journal of the Acoustical Society of America 72 (6), 1879–1890.

Freitas, R., Ricardo, F., Pereira, F., Sampaio, L., Carvalho, S., Gaspar, M., Quintino, V., Rodrigues, A.M., 2011. Benthic habitat mapping: concerns using a combined approach (acoustic, sediment and biological data). Estuarine, Coastal and Shelf Science 92, 598–606.

Freitas, R., Silva, S., Quintino, V., Rodrigues, A.M., Rhynas, K., Collins, W.T., 2003. Acoustic seabed classification of marine habitats: studies in the western coastal-shelf area of Portugal. ICES Journal of Marine Science 60, 599–608.

Hamilton, L.J., 2011. Acoustic seabed segmentation for echosounders through direct statistical clustering of seabed echoes. Continental Shelf Research 31, 2000–2011.

Hamilton, L.J., Mulhearn, P.J., Poeckert, R., 1999. Comparison of RoxAnn and QTC-view acoustic bottom classification system performance for the Cairns area, Great Barrier Reef, Australia. Continental Shelf Research 19, 1577–1597.

Hamilton, L.J., Parnum, I., 2011. Seabed segmentation from unsupervised statistical clustering of entire sonar backscatter curves. Continental Shelf Research 31 (2), 138–148.

Haris, K., Chakraborty, B., Ingole, B., Menezes, A., Srivastava, R., 2012. Seabed habitat mapping employing single and multi-beam backscatter data: a case study from the western continental shelf of India. Continental Shelf Research 48, 40–49.

Hastie, T., Tibshirani, R., Friedman, J., 2009. The Elements of Statistical Learning. Data Mining, Inference, and Prediction, second ed. Springer.

Hovland, M., 1983. Elongated depressions associated with pockmarks in the western slope of the Norwegian Trench. Marine Geology 51, 35–46.

Jackson, D.R., Richardson, M.D., 2007. High-Frequency Seafloor Acoustics. Springer, New York.

Jensen, A.C., Solberg, A.S., 2007. Fast hyperspectral feature reduction using piecewise constant function approximations. IEEE Geoscience and Remote Sensisng Letters 4 (4), 547–551.

Johnson, R.A., Wichern, D.W., 1988. Applied Multivariate Statistical Analysis, second ed. Prentice Hall, Englewood Cliffs, NJ.

Kohonen, T., 1990. The self-organizing map. Proceedings of the IEEE 78 (9), 1464–1480.

Madricardo, F., Tegowski, J., Donnici, S., 2012. Automated detection of sedimentary features using wavelet analysis and neural networks on single beam echosounder data: a case study from the Venice Lagoon, Italy. Continental Shelf Research 43, 43–54.

Medialdea, T., Somoza, L., León, R., Farrán, M., Ercilla, G., Maestro, A., Casas, D., Llave, E., Hernández-Molina, F.J., Fernández-Puga, M.C., Alonso, B., 2008. Multibeam backscatter as a tool for sea-floor characterization and identification of oil spills in the Galicia Bank. Marine Geology 249, 93–107.

Otto, L., Zimmerman, J.T.F., Furnes, G.K., Mork, M., Sætre, R., Becker, G., 1990. Review of the physical oceanography of the North Sea. Netherlands Journal of Sea Research 26 (24), 161–238.
Preston, J.M., 2005. Resampling Sonar Echo Time Series Primarily for Sediment Classification, US Patent 6801474.
Preston, J.M., 2009. Automated acoustic seabed classification of multibeam images of Stanton Banks. Applied Acoustics 70, 1277–1287.
Preston, J.M., Christney, A.C., Beran, L.S., Collins, W.T., 2004. Statistical seabed segmentation—from images and echoes to objective clustering. Proceedings of the Seventh European Conference on Underwater Acoustics (ECUA 2004), pp. 813–818.
Preston, J.M., Kirlin, R.L., 2003. Comment on 'Acoustic seabed classification: improved statistical method'. Canadian Journal of Fisheries and Aquatic Sciences 60, 1299–1300.
Rise, L., Olesen, O., Rokoengen, K., Ottesen, D., Riis, F., 2004. Mid-pleistocene ice drainage pattern in the Norwegian Channel imaged by 3D seismic. Quaternary Science Reviews 23, 2323–2335.
Rise, L., Rokoengen, K., 1984. Surficial sediments in the Norwegian sector of the North Sea between 60°30′ and 62°N. Marine Geology 58, 287–317.
Rise, L., Rokoengen, K., Skinner, A.C., Long, D., 1984. Nordlige Nordsjø. Kvartærgeologisk kart mellom 60°30′ og 62°N, og øst for 1°Ø. (Northern North Sea. Quaternary geology map between 60°30′ and 62°N, and east of 1°Ø) M 1:500.000. Institutt for kontinentalundersøkelser (IKU), Norway.
Roeder, K., Wasserman, L., 1997. Practical Bayesian density estimation using mixtures of normals. Journal of the American Statistical Association 92 (439), 894–902.
Rousseeuw, P.J., 1987. Silhouettes: a graphical aid to the interpretation and validation of cluster analysis. Journal of Computational and Applied Mathematics 20, 53–65.
Schwarz, G., 1978. Estimating the dimension of a model. Annals of Statistics 6 (2), 461–464.
Sejrup, H.P., Aarseth, I., Haflidason, H., Løvlie, R., Bratten, Å., Tjøstheim, G., Forsberg, C.F., Ellingsen, K.L., 1995. Quaternary of the Norwegian Channel: glaciation history and paleooceanography. Norsk geologisk tidsskrift 75 (2–3), 65–87.
Sigmond, E.M.O., 2002. Geologisk kart over land-og havområder i Nordeuropa, målestokk 1:4.000.000. Norges geologiske undersøkelse.
Snellen, M., Siemens, K., Simons, D.G., 2011. Model-based sediment classification using single-beam echosounder signals. Journal of the Acoustical Society of America 129 (5), 2878–2888.
Sternlicht, D.D., De Moustier, C.P., 2003. Remote sensing of sediment characteristics by optimized echo-envelope matching. Journal of the Acoustical Society of America 114 (5), 2727–2743.
Theodoridis, S., Koutroumbas, K., 2009. Pattern Recognition, fourth ed. Academic Press.
Van Vossen, R., Eidem, E.J., Ivansson, S., Chalindar, B., Dybedal, J., Colin, M.E.G.D., Benders, F.P.A., Andersson, B.L., Juhel, B., Cristol, X., Olsen, G.-K., Pihl, J.N.B., Tveit, E., Jespers, S., Ainslie, M.A., 2013. Improved active sonar tactical support by through-the-sensor estimation of acoustic seabed properties. IEEE Journal of Oceanic Engineering (to be published).
Van Walree, P.A., Ainslie, M., Simons, D.G., 2006. Mean grain size mapping with single-beam echo sounders. Journal of the Acoustical Society of America 120 (5), 2555–2566.
Van Walree, P.A., Tegowski, J., Laban, C., Simons, D.G., 2005. Acoustic seafloor discrimination with echo shape parameters: a comparison with ground truth. Continental Shelf Research 25, 2273–2293.
Von Szalay, P.G., McConnaughey, R.A., 2002. The effect of slope and vessel speed on the performance of a single beam acoustic seabed classification system. Fisheries Research 54 (2), 181–194.
Wessel, P., Smith, W.H.F., 1991. Free software helps map and display data. Eos Transactions American Geophysical Union 72.
Wienberg, C., Bartholomä, A., 2005. Acoustic seabed classification in a coastal environment (outer Weser Estuary, German Bight)-a new approach to monitor dredging and dredge spoil disposal. Continental Shelf Research 25 (9), 1143–1156.
Winther, N.G., Johannessen, J.A., 2006. North Sea circulation: Atlantic inflow and its destination. Journal of Geophysical Research-Oceans 111, C12018, doi:10.1029/2005JC003310.